RL-TR-96-196
Final Technical Report
December 1996

MONOLITHIC P - I - n MULTIPLE QUANTUM WELL (MQW) PHOTOREFRACTIVE DEVICES

CoreTek, Inc.

Parviz Tayebati and Christos Hantzis

19970211 021

APPROVED FOR PUBLIC RELEASE; DISTRIBUTION UNLIMITED.

DTIC QUALITY INSPECTED 3

Rome Laboratory
Air Force Materiel Command
Rome, New York

This report has been reviewed by the Rome Laboratory Public Affairs Office (PA) and is releasable to the National Technical Information Service (NTIS). At NTIS it will be releasable to the general public, including foreign nations.

RL-TR-96-196 has been reviewed and is approved for publication.

APPROVED:
GEORGE BROST
Project Engineer

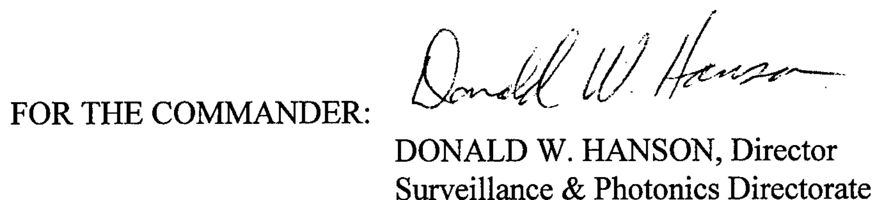

FOR THE COMMANDER:
DONALD W. HANSON, Director
Surveillance & Photonics Directorate

If your address has changed or if you wish to be removed from the Rome Laboratory mailing list, or if the addressee is no longer employed by your organization, please notify RL/OCPA, 25 Electronic Pky, Rome, NY 13441-4514. This will assist us in maintaining a current mailing list.

Do not return copies of this report unless contractual obligations or notices on a specific document require that it be returned.

REPORT DOCUMENTATION PAGE

Form Approved
OMB No. 0704-0188

Public reporting burden for this collection of information is estimated to average 1 hour per response, including the time for reviewing instructions, searching existing data sources, gathering and maintaining the data needed, and completing and reviewing the collection of information. Send comments regarding this burden estimate or any other aspect of this collection of information, including suggestions for reducing this burden, to Washington Headquarters Services, Directorate for information Operations and Reports, 1215 Jefferson Davis Highway, Suite 1204, Arlington, VA 22202-4302, and to the Office of Management and Budget, Paperwork Reduction Project (0704-0188), Washington, DC 20503.

1. AGENCY USE ONLY *(Leave blank)*	2. REPORT DATE	3. REPORT TYPE AND DATES COVERED
	December 1996	**FINAL, May 95 - May 96**

4. TITLE AND SUBTITLE
MONOLITHIC P- I - n MULTIPLE QUANTUM WELL (MQW) PHOTOREFRACTIVE DEVICES

5. FUNDING NUMBERS
C - F30602-95-C-0139
PE - 62702F
PR - 4600
TA - P4
WU - PT

6. AUTHOR(S)
Parviz Tayebati, Christos Hantzis

7. PERFORMING ORGANIZATION NAME(S) AND ADDRESS(ES)
CoreTek, Inc.
3 Preston Court
Bedford MA 01730

8. PERFORMING ORGANIZATION REPORT NUMBER
N/A

9. SPONSORING / MONITORING AGENCY NAME(S) AND ADDRESS(ES)
Rome Laboratory/OCPA
25 Electronic Pky
Rome NY 13441-4515

10. SPONSORING / MONITORING AGENCY REPORT NUMBER
RL-TR-96-196

11. SUPPLEMENTARY NOTES
Rome Laboratory Project Engineer: George Brost, OCPA, (315) 330-7669

12a. DISTRIBUTION AVAILABILITY STATEMENT
APPROVED FOR PUBLIC RELEASE; DISTRIBUTION UNLIMITED

12b. DISTRIBUTION CODE

13. ABSTRACT *(Maximum 200 words)*
In this paper we report a monolithic p-i-n multiple quantum-well (MQW) GaAlAs photorefractive device operating in reflection mode. The device structure consists of a photorefractive structure grown with low temperature grown (LTG)-GaAlAs charge blocking layers on top of a 20 period n-type GaAlAs/AlAs quarter wave stack mirror. The device operates by double passing mutually coherent beams through the photorefractive structure exhibiting nearly 0.23% input diffraction efficiency. The writing energy of approximately 20nJ/cm^2 is nearly seven (7) times better than those of previously reported devices.

14. SUBJECT TERMS
Photorefractive devices, Multiple quantum wells (MQW), Low temperature grown GaAlAs

15. NUMBER OF PAGES
20

16. PRICE CODE

17. SECURITY CLASSIFICATION OF REPORT	18. SECURITY CLASSIFICATION OF THIS PAGE	19. SECURITY CLASSIFICATION OF ABSTRACT	20. LIMITATION OF ABSTRACT
UNCLASSIFIED	**UNCLASSIFIED**	**UNCLASSIFIED**	**UNLIMITED**

NSN 7540-01-280-5500

Standard Form 298 (Rev. 2-89)
Prescribed by ANSI Std. Z39-18
298-102

DTIC QUALITY INSPECTED 3

Table of Contents

1. INTRODUCTION **1**

2. DESIGN, GROWTH AND FABRICATION OF DEVICES **1**

3. ELECTRICAL AND OPTICAL TESTING OF DEVICES **2**

3.1 Diffraction efficiency 2
3.2 Voltage dependence 3
3.3 Transient electroabsorption 4
3.4 Scaling of device response time with optical intensity 5

LIST OF FIGURES

Fig. 1. Applied step voltage and transient photorefractive diffraction 7
Fig. 2. Input diffraction efficiency as function of reverse voltage 7
Fig. 3. Wavelength dependence of output diffraction efficiency 8
Fig. 4. Wavelength dependence of the diffraction efficiency 8
Fig. 5. Intensity dependence of the half rise time 9

1. INTRODUCTION

Photorefractive epitaxial devices are band-gap engineered, high speed, real-time holograms that operate by a combination of charge transport and resonant electrooptic nonlinearties in semiconductors. Operating with response times on the order of 1μs these devices allow high dynamic range image processing such as optical correlation with data through puts nearing 10^{12}/s. The earliest version of these devices using the quantum confined Stark effect consisted of a MQW film sandwiched between two buffer SiO_2 or Si_3N_4 layers and appropriate transparent electrodes.[1,2] These devices are however quite difficult to fabricate since the process involved a two layer film deposition after growth, followed by substrate removal and deposition of two more films and appropriate metalization. In order to solve this problem we showed that wide gap LTG GaAlAs could replace oxide or nitride charge blocking (CB) layers resulting in nearly monolithic devices[3] with over 3% output diffraction efficiency, although these devices still required substrate (GaAs) removal as a part of the process, a costly fabrication step. In reference 3 we demonstrated devices with intrinsic MQWs and bulk thin films of LTG-GaAlAs as electrooptic medium.[2] Based on these findings Lahiri et al.[4] showed that normally grown GaAlAs CB layers in combination with Low Temperature Grown MQWs could result in similar performance.

2. DESIGN, GROWTH AND FABRICATION OF DEVICES

In this work we report successful demonstration of a monolithic photorefractive device by growing MQW photorefractive device structure on a GaAlAs/AlAs quarter-wave stack mirror. In addition to being monolithic, the proposed device has the potential of operating at lower voltages and higher diffraction efficiencies by doubling the effective interaction length. The device structure described as follows was grown by Molecular

Beam Epitaxy on 3 inch n^+-GaAs substrate: 1000Å n^+ (1×10^{18} cm^{-3}) GaAs as buffer, 20 periods of n^+ ($1\times10^{18}cm^{-3}$) AlAs(738Å)/$Ga_{0.9}Al_{0.1}As$(600Å) quarter-wave stack mirror, 6000Å of LTG- $Ga_{0.7}Al_{0.3}As$ as CB layer , 121 periods of AlAs(30Å)/GaAs(95Å) ultra-narrow-barrier MQW, [5] 6000Å of LTG-$Ga_{0.7}Al_{0.3}As$ as CB layer and 5000Å p^+ ($5\times10^{18}cm^{-3}$)-$Ga_{0.7}Al_{0.3}As$ as top electrode layer capped with 50Å p^+ (5×10^{18} cm^{-3})-GaAs. As such the device was designed to exhibit a heavy-hole exciton at 840nm and a mirror stack centered at 850nm allowing for approximately 10nm exciton red-shift under the applied voltage. Substrate temperatures used were 325°C (set by thermocouple) for the low temperature (Al,Ga)As layers, and 600°C (set by infra-red pyrometer) for all other layers. As/Group III Beam Equivalent Pressure (BEP) ratios, as measured with an ion gauge in the growth position, were 12:1 for the low temperature (Al,Ga)As layers, but considerably higher for the Bragg reflectors and p^+ top layer (~28-34). From the grown wafer a number of 7mm× 7mm devices were fabricated by cleaving followed by a large mesa formation by etching only the p^+ layer around the periphery of the chip down to the LTG layer. The devices were Al metalized and electrodes were connected using silver paste. Although we tested devices from various locations in the wafer here we only report the response of devices from the 1cm radius at the center of the wafer marked as A or just outside this region marked as AB.

3. Electrical and Optical Testing of Devices

3.1 Diffraction Efficiency

Using an Ar^+ pumped Ti: Sapphire laser as the laser source and a digital storage oscilloscope we measured the transient electroabsorption, diffraction efficiency, intensity dependence and incidence angle variation of the photorefractive effect in these devices. All the data presented in this paper were measured at a grating spacing of 40μm with laser beams polarized in the plane of incidence. The devices operate as follows: as soon as a step reverse voltage is applied photogenerated carriers in the bright regions of MQW drift

towards the CB layer and are eventually trapped at the LTG interface causing a screening of the electric field in the MQW region. In the dark regions also a similar effect occurs although at much slower rates. The screening of the field in the bright areas create an electric field grating and a corresponding quantum confined stark effect electroabsorption and electrorefractive grating patterns replicating the interference pattern. The readout beam(s) (here the writing beams themselves) are then diffracted from the grating. In Figure 1 the time evolution of the diffraction efficiency is shown in response to a 10V to -40V step voltage. The I-V curve shown in the insert in Figure 2 shows a clear reverse breakdown voltage of nearly -45V indicating the maximum applicable voltage. Although in all A and AB devices we observed a single diffracted peak (in time) independent of wavelength, in some devices towards the edge we observed splitting of the single peak into two peaks and then back to a single broader peak as the wavelength was scanned from 848nm to 853nm. We also evaluated the response of the device as a function of the frequency. We observed no change in the shape of the transient diffraction as the period of the applied step voltage was decreased to nearly half the length of the diffracted signal (~50μs). The results were in conflict with observations in references 3 and 4 where charge trapping in the LTG layers were suspected of causing a highly pulse-width dependent photorefractive response. It is however quite possible that in these samples the density of the Arsenic precipitates are not as high as those in reference 3 and 4 possibly because of different growth conditions.

3.2 Voltage Dependence of Diffraction Efficiency

In Figure 2 we show the input diffraction efficiency[6] writing as a function of voltage at 849nm and at 30° incident angle where the diffraction efficiency was maximum (in device AB5). In these experiments a maximum input diffraction efficiency of 0.23% corresponding to an output diffraction efficiency [6] of 0.29% were measured. Note that

the diffraction efficiency saturates beyond the breakdown voltage and increases exponentially below this level. The exponential increase of the diffraction efficiency as a function of voltage explains the delay between the applied step voltage and the onset of diffraction in Figure 1. The $1/e^2$ maximum diffraction efficiency occurs at a reverse voltage of approximately -35V indicating a clear "turn-on" behavior. This voltage is required to fully deplete the nominally intrinsic grown MQW region before a photoinduced grating can be generated. From this voltage we calculate a background carrier density of 1×10^{16} which is rather high but feasible since this structure was grown immediately after reloading the MBE system. In order to test this hypothesis and increase the diffraction efficiency we are now in the process of implanting samples of the same wafer with H^+ ions to reduce the background carrier density and therefore the turn-on voltage. The large depletion voltage may also explain the relatively low value of the diffraction efficiency the voltages required to reduce the dark carrier density to below the photoinduced carrier concentration level throughout the MQW region ($\sim10^{12}$ cm^{-3} at $10mw/cm^2$) cause a significant Stark shifting of the exciton before any charge screening can occur. Furthermore note in Figure 2 that the diffraction efficiency saturates for voltages above 40V also corresponding to the avalanche breakdown voltage shown in the I-V curve in the insert in Figure 2. We speculate that for voltages beyond avalanche, the grating formation is adversely affected by the spatially uniform amplified dark current.

3.3 Transient Electroabsorption

The spectral response of the peak diffraction efficiency as well as the peak transient change in reflection $\Delta R/R$ are shown in Figure 3. The transient change in reflectance occurs as charges move towards the CB layers to screen the field under a step voltage. A complete recovery of reflectivity to its value before the step voltage points to the effectiveness of the CB layers in blocking the photoinduced charges and successfully

screening the entire electric field. In many instances however we observed only partial recovery of reflectance depending on all important factors including intensity, voltage and wavelength. Initial transient photocurrent measurements also showed a transient photocurrent and a finite DC photocurrent indicating imperfect charge screening by the CB layers.

Figure 3 shows the change in peak reflectivity $\Delta R/R$ oscillates about zero as a function of wavelength whereas at longer wavelengths it is only negative. These results confirm a heavy hole exciton peak at 840nm exactly as designed. The peak diffraction efficiency in this device (A5) at -40V occurs well below the exciton peak at 855nm, however, as shown in Figure 4.a, the diffraction spectrum depends highly on the angle of incidence of the writing beams. In Figure 4.a and b we show the spectral diffraction efficiency and reflectance of another device (A7) in the same region of the wafer at various incidence angles at -30V applied voltage. Note the significant increase and spectral shift of diffraction efficiency with increasing angle in this device because of Fabry-Perot effects. In particular an output diffraction efficiency of up to 0.5% is obtained at 60° incidence angle at this voltage. This coincides with a sharp drop in zero-field reflectivity as show in Figure 4.b.

3.4 Scaling of Device Response Time with Optical Intensity

The speed of the photorefractive device was also investigated as a function of peak incident intensity (I_o) of the writing Gaussian beams. The results for two different samples (A7 and A8) for incident angle of 45° are shown in Figure 5. In these experiments a NIST traceable power meter was used to measure the total power and a 1-D Reticon detector array was used to measure the Gaussian beam profile at the location of the device. The half-width-half-maximum of Gaussian beam was found to be 1.32mm

at this point. The half-rise time fits very well to I^{-x} with x=1 in both cases. In both devices we observed a saturation of the response time at 1 to 2μs as the intensity was increased beyond $10mW/cm^2$. The saturating limiting response time could be explained in terms of the RC time constant of the devices or the switching speed of our high voltage function generator. The I^{-1} behavior as well as intensity independent diffraction efficiency is consistent with the standard models of photorefractive effect assuming a linear photoconducitvity behavior.[7] The energy necessary for writing a photorefractive grating with 2ms response time at $10mW/cm^2$ is $20nW/cm^2$. This is approximately 40 times faster than previously reported energy ($840nw/cm^2$) for writing a photorefractive grating in the earliest form of these devices [2] using 100ÅGaAs / $100ÅGa_{0.7}Al_{0.3}As$ MQWs. However, we must also note that the 1.5% input diffraction efficiency in the device presented in reference 2 is six (6) times larger than the maximum diffraction efficiency in our devices. This may mean that if the diffraction efficiency could be increased to the same level as in reference 2, for example by ion implantation, the writing energy efficiency will be only seven (7) time better than that in reference 2.

Future studies of similar devices implanted by hydrogen ions and shallow quantum wells are now under progress and will be published separately. We would like to thank G. A. Brost for support of this work under a contract (# F30602-95-c-0139) from Rome Labs.

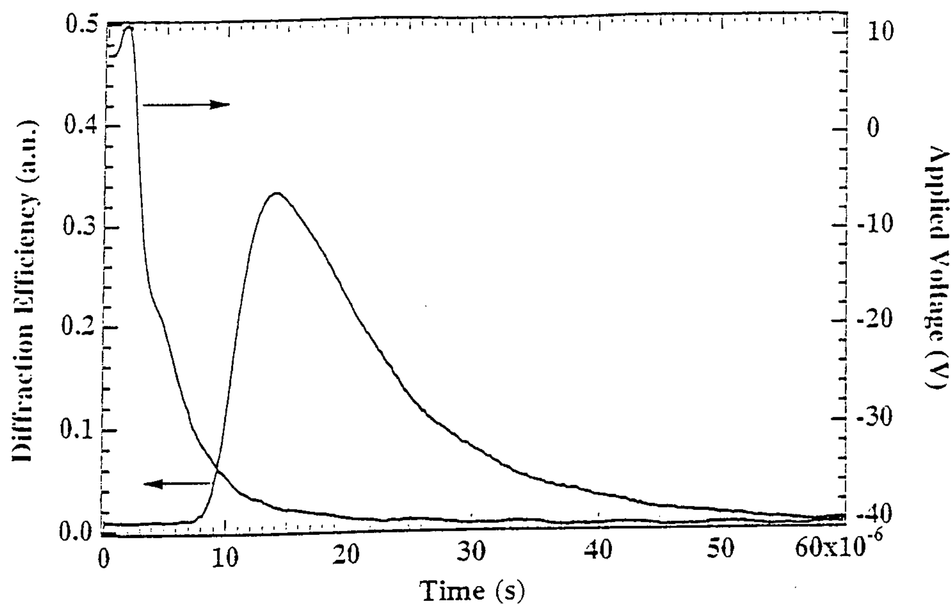

Figure 1. Applied step voltage and transient photorefractive diffraction

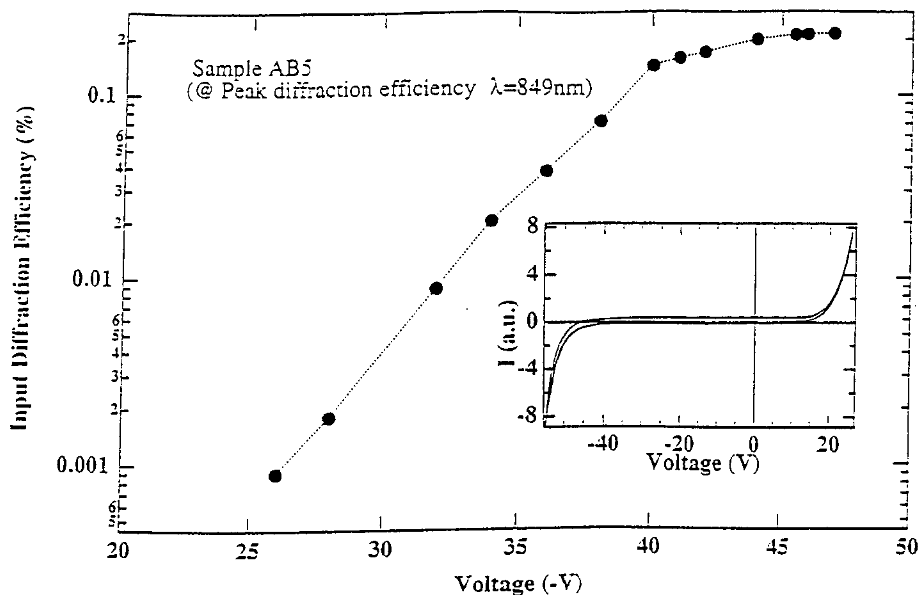

Figure 2. Input diffraction efficiency as a function of reverse voltage. Insert show is a typical I-V curve for (A) devices.

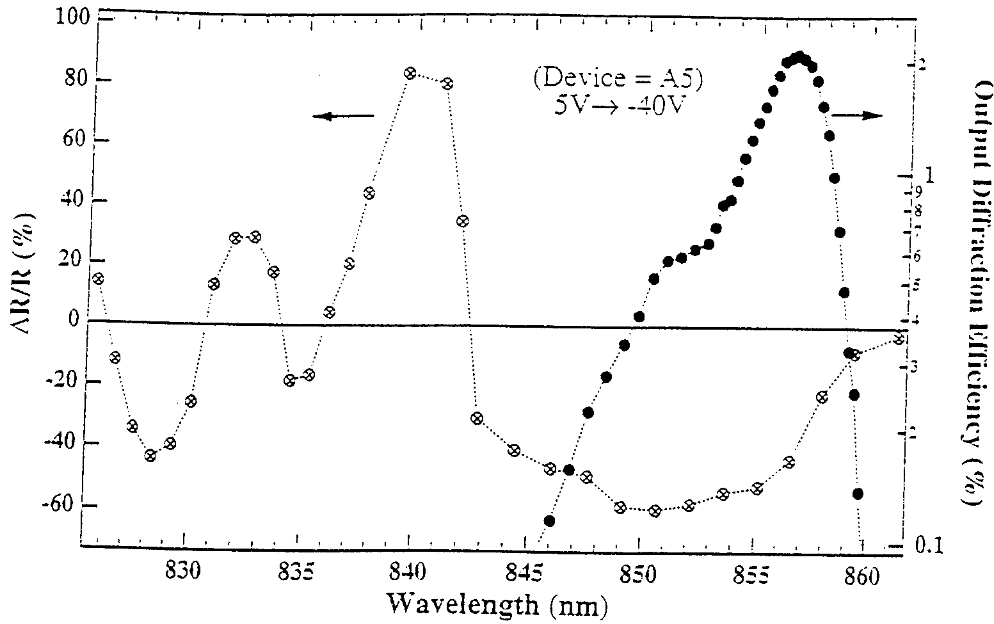

Figure 3. Wavelength dependence of the output diffraction efficiency (at -40V) and transient change in reflectivity.

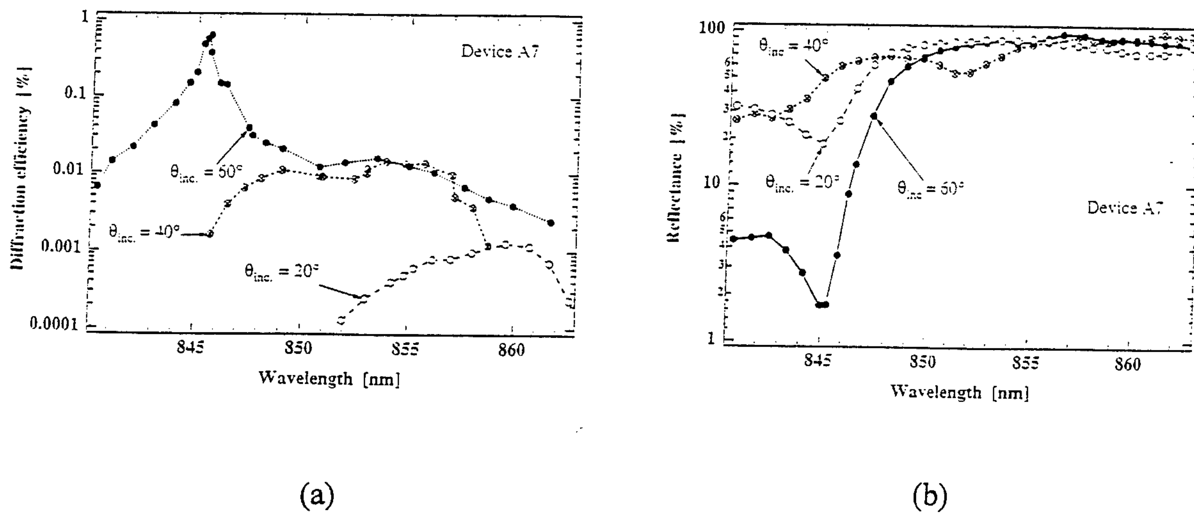

Figure 4. (a) Wavelength dependence of the diffraction efficiency (at -32V) at different angles of incidence and (b) corresponding reluctance spectra.

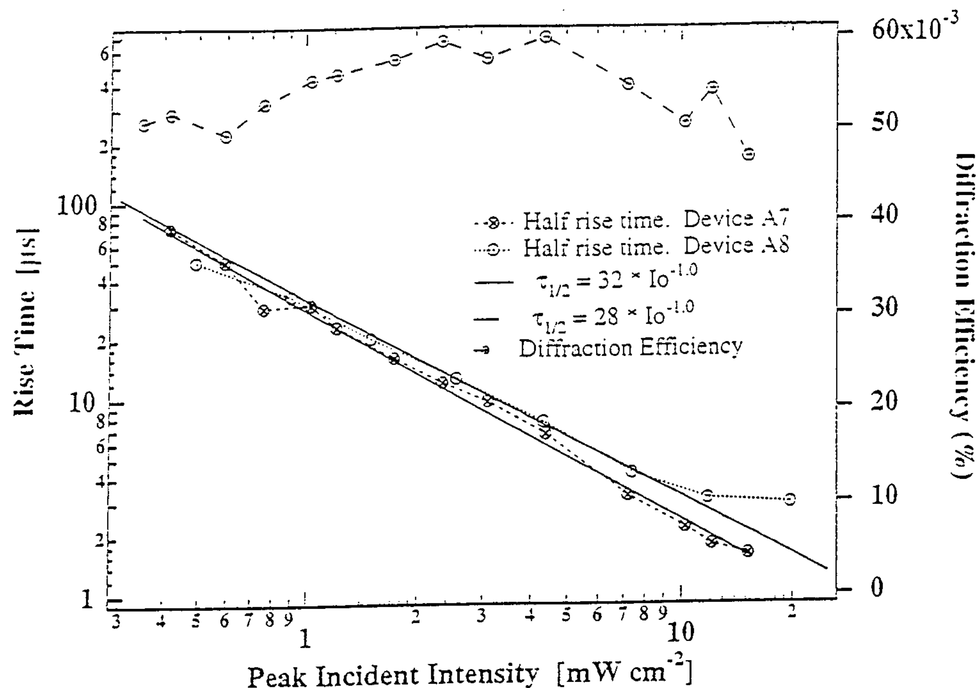

Figure 5. Intensity dependence of the half rise time and the diffraction efficiency.

---

[1] A. M. Glass, D. D. Nolte, D. H. Olson, G. E. Doran, D. S. Chemla and W. H. Knox, Opt. Lett. 15, 264 (1990)

[2] A. Partovi, A. M. Glass, O. H. Olson, G. J. Zydzik, H. M. O'Bryan, T. H. Chiu and W. H. Knox Appl. Phys. Lett. 62(5), p. 4641 Feb. 1993

[3] P. Tayebati, K. Krishnaswami, D. D. Nolte and M. R. Melloch, Technical Digest, OSA, Topical Meeting on Photorefractive Materials, Effects and Devices, June 1995, P. 536

[4] I. Lahiri, K. M. Kwolek, D. D. Nolte and M. R. Melloch, Appl. Phys. Lett. 67 (10), P.1408

[5] K. W. Goossen et al. Appl. Phys. Lett. 57 (24), p. 2582, (1990)

[6] "Input diffraction efficiency" is defined as the peak power in the first order diffracted beam divided by the input power of the corresponding beam and the "Output diffraction efficiency" is defined as the peak power in the first order diffracted beam divided by the output power of the writing beam.

[7] See Tayebati and Mahgerefted and references within for a comprehensvie I^x issue in photorefractive materials.

☆U.S. GOVERNMENT PRINTING OFFICE: 1997-509-127-47083

MISSION

OF

ROME LABORATORY

Mission. The mission of Rome Laboratory is to advance the science and technologies of command, control, communications and intelligence and to transition them into systems to meet customer needs. To achieve this, Rome Lab:

a. Conducts vigorous research, development and test programs in all applicable technologies;

b. Transitions technology to current and future systems to improve operational capability, readiness, and supportability;

c. Provides a full range of technical support to Air Force Materiel Command product centers and other Air Force organizations;

d. Promotes transfer of technology to the private sector;

e. Maintains leading edge technological expertise in the areas of surveillance, communications, command and control, intelligence, reliability science, electro-magnetic technology, photonics, signal processing, and computational science.

The thrust areas of technical competence include: Surveillance, Communications, Command and Control, Intelligence, Signal Processing, Computer Science and Technology, Electromagnetic Technology, Photonics and Reliability Sciences.